Bulletin of Glacier Research 15 (1997) *59−69*

Hydrodynamic effects on the basin expansion of Tsho Rolpa Glacier Lake in the Nepal Himalaya

Kazuhisa CHIKITA[1], Tomomi YAMADA[2], Akiko SAKAI[3] and Ram P. GHIMIRE[4]

1 Division of Earth and Planetary Sciences, Graduate School of Science, Hokkaido University, Sapporo, 060 Japan

2 Institute of Low Temperature Science, Hokkaido University, Sapporo, 060 Japan

3 Institute for Hydrospheric-Atmospheric Sciences, Nagoya University, Nagoya, 464-01 Japan

4 Water and Energy Commission Secretariat (WECS), Ministry of Water Resources, Kathmandu, Nepal

(Received March 21, 1997 ; Revised manuscript received April 14, 1997)

Abstract

In order to clarify the physics of basin expansion of a supraglacial lake, we investigated the meteorology, hydrodynamics and basin topography in Tsho Rolpa Glacier Lake (27°51′N, 86°29′E : lake level, 4580 m above sea level ; length, about 3 km ; surface area, 1.39 km^2 ; maximum depth, 131 m) in the premonsoon season of 1995. Tsho Rolpa Lake has been expanded by a large recession of the glacier (the Trakarding Glacier) since 1950's, when it was about 1 km long accompanied by six closed ponds 100 to 200 m long. The rapid lake basin expansion accompanying the glacier recession is probably due to an increase of meltwater discharge from the global warming. Vertical and continuous measurements of water temperature and suspended sediment concentration (SSC) in the lake revealed that under the density stratification made up by large SSC, thermal conditions at the bottom are controlled by dynamic behaviors of *sediment-laden underflows* and *wind-driven currents*. The underflows were generated off a subaqueous mouth of englacial tunnels, which is located at the base of the cliff-shaped glacier terminus. The leeward transport of radiative heat by wind-driven currents is responsible for enhancing the ice carving at the glacier terminus ; a receding speed of the terminus was 18 cm/d on average in 1993−1994, being 280 times as high as the rate of lake-bottom subsidence, 0.064 cm/d at uplake of the terminal moraine.

1. Introduction

In the Nepal Himalaya, some moraine-dammed supraglacial lakes 1−3 km long exist on the termini of debris-covered glaciers. In the 1950's, each of the lakes was scaled down to one or a few closed ponds of the order 100 m in length on the glacier terminus. By one time the ponds have grown into an open lake, still expanding at present. The lake expansion is caused by the recession of the glacier, possibly due to the recent global warming. Since 1964, it has often been recorded that some glacier lake bursts by the collapse of a terminal moraine (Yamada, 1993, 1996). The flood caused by the lake burst, called GLOF (Glacier Lake Outburst Flood), has given serious damage to hydropower plants, people, houses, trails, livestock, etc. in the downstream area. The terminal and side moraines partially involve the glacial ice even after the glacier recession. The moraines are thus unstable and fragile in structure, because they are always in direct contact with the lake water more than 0°C.

In order to clarify the physics of the lake basin expansion, we investigated the meteorology, hydrodynamics and basin topography of Tsho Rolpa Lake in the premonsoon of May 1995 (Fig. 1). Tsho Rolpa Lake appears to exhibit the high potentiality of GLOF, because the lake is dammed up only by the terminal moraine partially involving the ice ; its lateral expansion is likely to be almost achieved, since either side of the lake basin is bordered by the lateral moraines involving a little amount of fossil ice.

According to a history of the basin expansion of

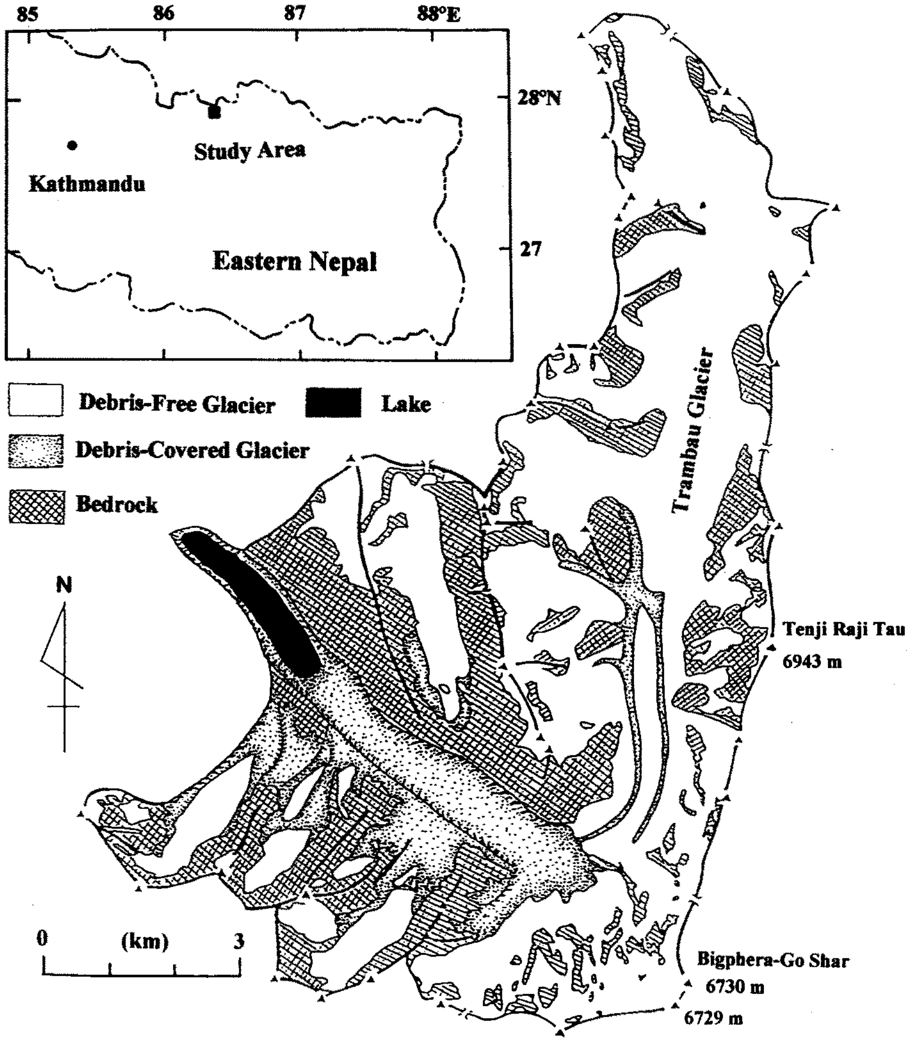

Fig. 1. Location of Tsho Rolpa Glacier Lake and its drainage basin. The lake is developed on the terminus of the debris-covered Trakarding Glacier (Lower Trambau Glacier) (modified after Sakai, 1995).

Tsho Rolpa Lake for 1958–1990 (Mool *et al.*, 1993), in 1958 there existed one lake about 1 km long and six ponds about 100 to 200 m long on the glacier terminus. In 1968, the lake expanded into a big lake by merging the upper ponds. During 1968–72, the lake expansion was rather low, but since 1974 or 1975–77, the lake area has increased especially upstream, *i.e.* indicating the great recession of the glacier terminus. The increased glacier recession could correspond to an increase of annual mean air temperature over the earth since about 1975, representing the global warming (*e.g.*, Jones *et al.*, 1986).

According to the request of Water and Energy Commission Secretariat (WECS), Ministry of Water Resources, Nepal, T. Yamada and T. Kadota were dispatched in 1992–1996 as JICA (Japan International Cooperation Agency) Glaciology Expert. They started to research in Tsho Rolpa Lake in 1993. In this study, the lake hydrodynamics will be especially emphasized to clarify the relationship between thermal conditions on the lake bottom and a lake-current system.

2. Study Area and Methods

Tsho Rolpa Lake (27°51′N, 86°29′E) is located at 110 km east-northeast of Kathmandu and developed on the terminus of the Trakarding Glacier (or the Lower Trambau Glacier) (Fig. 1). A bathymetric map of the lake (Fig. 2) was obtained from T. Kadota's plumbing in 1994 (Kadota, 1994). The lake about 3 km long and 0.5 km wide has the surface area of 1.39 km^2 and maximum and mean depths of 131 m and 55.1 m, respectively in the drainage area of 77.6 km^2. The lake is bordered by the terminal moraine at the downlake end, the lateral moraine (slope angle, 25−80°) 40−100 m high on either side and the cliff-shaped glacier terminus about 25 m high at the uplake end (Kadota, 1994, Sakai, 1995). Part of the terminal moraine involves the fossil ice (Yamada, 1996). The lake bottom basin is covered by the glacial debris and more fine-grained lacustrine sediment. The fossil ice below the bottom sediments possibly increases in volume from the deepest point toward the glacier terminus or the terminal moraine (Fig. 2). Debris-free and debris-covered glaciers occupy 55.3 % and 16.5 % of the drainage area (77.6 km^2), respectively (Sakai, 1995). The highest peak in the drainage basin is Mt. Tenji Ragi Tau (6943 m asl) (Fig. 1). The geology of the drainage basin consists of Precambrian to Mesozoic metamorphic, sedimentary and intrusive rocks.

Fig. 2 shows site locations on the bathymetric map for observation in the premonsoon season of May 1995. At each of sites A (midlake) and G (near the glacier terminal cliff), in order to obtain time series of water temperature, we fixed temperature data loggers (Alec Electronics, Inc., model MDS-T ; accuracy, ±0.15 °C) at depths of 0.1 m and 20 m, at the bottom and at 1 m above the bottom. The data logging was performed at 1 min intervals. In order to examine interrelations among various lake currents, the spectral analysis by the FFT (Fast Fourier Transform) method was carried out for the time series of water temperature.

At sites A, B, C, D, E, G and G', vertical profiles of water temperature and turbidity were obtained by lowering on a boat the Temperature Profiler (Alec Electronics, Inc., model ABT-1 : accuracy, ±0.05 °C) and a turbidimeter of infrared back scattering type (Alec Electronics, Inc., model MTB-16K : range, 0−2000 mg/l ; accuracy, ±40 mg/l). The turbidity (T_b) values were converted into suspended sediment concentration, C (mg/l) obtained by filtering simultaneously sampled water. Two regression lines, $C = 0.3846 T_b$ ($0 \leqq T_b \leqq 529.5$ mg/l ; $r^2 = 0.882$) and $C = 0.8706 T_b - 257.4$ ($529.5 < T_b \leqq 2000$ mg/l ; $r^2 = 0.886$) were employed to the conversion. Meteorological conditions (air temperature, relative humidity, air pressure, wind velocity, solar radiation and rainfall) were observed at 1 h intervals at site M on an islet. At site R (outlet), water level was likewise monitored with a pressure gauge (accuracy, ±1 cm). The water discharge was measured frequently on a bridge with an electromagnetic current meter. The consequent stage-discharge rating curve was sufficiently stable for the duration of previous and present studies as compiled by Yamada (1996). The receding rate of the cliff-shaped glacier terminus has frequently been observed since September 1993 by T. Yamada, T. Kadota and A. Sakai.

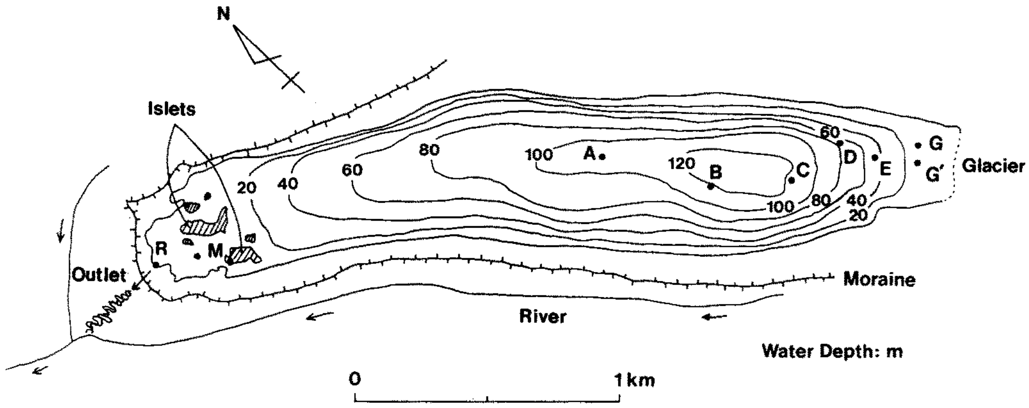

Fig. 2. Location of observation sites on a bathymetric map made up by Kadota (1994).

3. Results and Discussion

3-1. Meteorological Conditions

Fig. 3 shows time series of meteorological data recorded at site M for a period 1 May to 27 May 1995. It is seen that precipitation was rather small in the premonsoon season of 1995 and that wind speed, air temperature and solar radiation exhibited clear diurnal variations. The weak rainfalls of 11–19 May were probably caused by the advection of wet air mass in the upvalley direction during the passage of weak depressions. Meantime the solar radiation, however, did not decrease considerably. This indicates the stable supply of radiative heat unique for the lake warming. The solar radiation is mostly absorbed at the lake surface because of the low transparency less than 0.2 m or the high turbidity of lake water (Yamada, 1996).

The air pressure varies semi-diurnally with maximums at about 11 : 00 and 22 : 00 and with minimums at about 3 : 00 and 15 : 00. The wind behaviors correspond to the variation of air pressure ; a weak mountain (southeast to south-southeast) wind blew typically at less than 1 m/s during the increased air pressure at 3 : 00–8 : 00, while a relatively strong valley (northwest to north-northwest) wind prevailed at 2–7 m/s during the decreased pressure at 10 : 00 – 19 : 00. These winds thus blew in the longitudinal direction over the lake (see Fig. 2). The mountain wind is probably a local katabatic wind produced on the Upper Trambau Glacier, whereas the valley wind is possibly due to the upslope air advection of large scale in the Himalaya. It should be noted that the strong valley wind blows toward the glacier terminal cliff which contacts directly with the lake water. This wind may produce advanced wind waves at the surface and wind-driven currents in the surface layer. The wind-driven currents are likely to transport the radiative heat toward the terminal cliff, thus being responsible for the subaqueous glacier-melt.

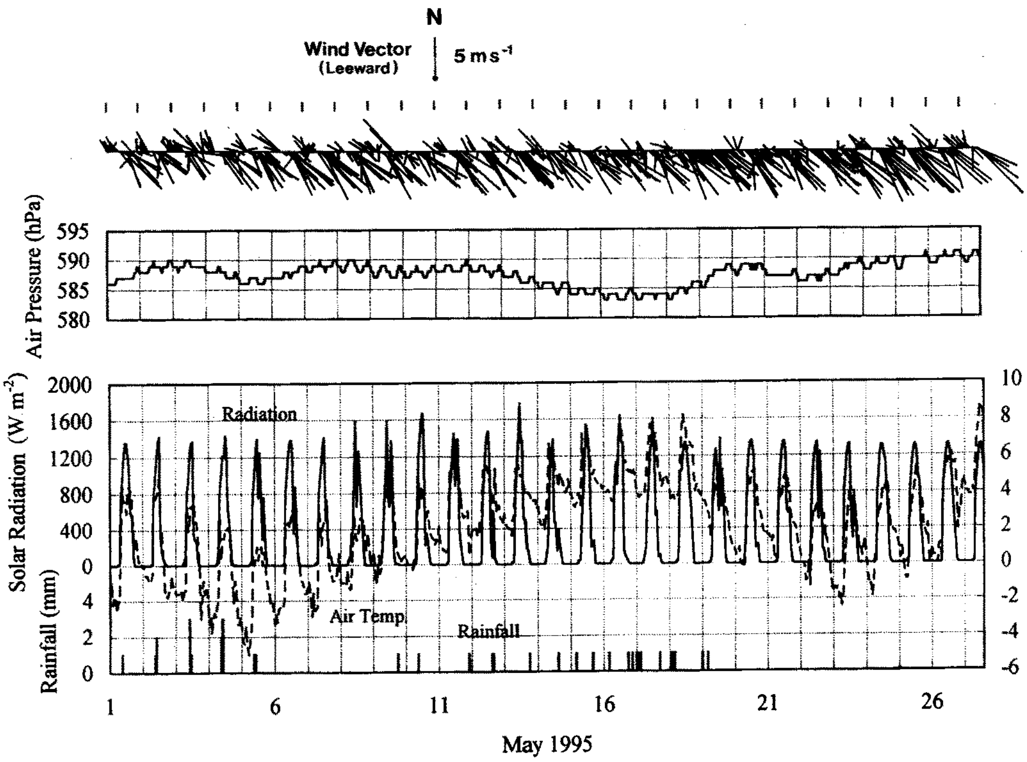

Fig. 3. Meteorological conditions observed at site M for 1–27 May 1995. Wind vectors indicate leeward directions from the observation point (site M), *i.e.* directions of wind forcing over the lake.

3-2. Vertical Profiles of Water Temperature and Suspended Sediment Concentration

Fig. 4 shows vertical distributions of water temperature, T, suspended sediment concentration (SSC), C and density *in situ*, σ at sites B, G and G'. σ was calculated by $\sigma=(\rho-1000)\times 10$, where ρ is water density (kg/m³) at C mg/l and T °C, given by $\rho=(1-C\times 10^{-3}/\rho_s)\cdot\rho_T+C\times 10^{-3}$ (ρ_s, suspended particle density, 2650 kg/m³ for Tsho Rolpa Lake ; ρ_T, clear water density at T °C). Dissolved solids concentration of lake water is here negligible because of its slight amount less than 1 mg/l, thus being within the SSC accuracy, ± 15 mg/l (the turbidity accuracy ± 40 mg/l multiplied by 0.3846 in the given T_b-C relation for $0\leqq T_b\leqq 529.5$ mg/l).

The water temperature profile at site B near the deepest point (Fig. 4a) indicates that the lake has an isothermal (about 5 °C) mixed layer at depths less than 10 m with the thermocline at about 13 m in depth. The temperature gradually decreases from 3.2 °C at a depth of 15 m to 2.6 °C near the bottom. The SSC distribution is rather complicated, showing a small range of 121−152 mg/l at depths less than 15 m and an increase at more depths with six local maximums. The σ profile is similar to that of SSC, because the water density depends on SSC rather than temperature. As a result, an almost isopycnal layer exists at depths of 0−35 m. The isothermal layer and the lower metalimnion (layer with a relatively great change in temperature) at depths less than 25 m could be produced by the turbulent mixing from the wind shear, while the relatively cold isopycnal layer at 25−35 m in depth was probably generated by *density interflows* horizontally moving from near the glacier terminus toward the terminal moraine. The SSC increases at depths more than 35 m, especially at more than 100 m with a peaked value of 740 mg/l at 5 m above the bottom. The temperature decrease is relatively great at depths more than 110 m with being pycnally unstable at depths of more than 115 m.

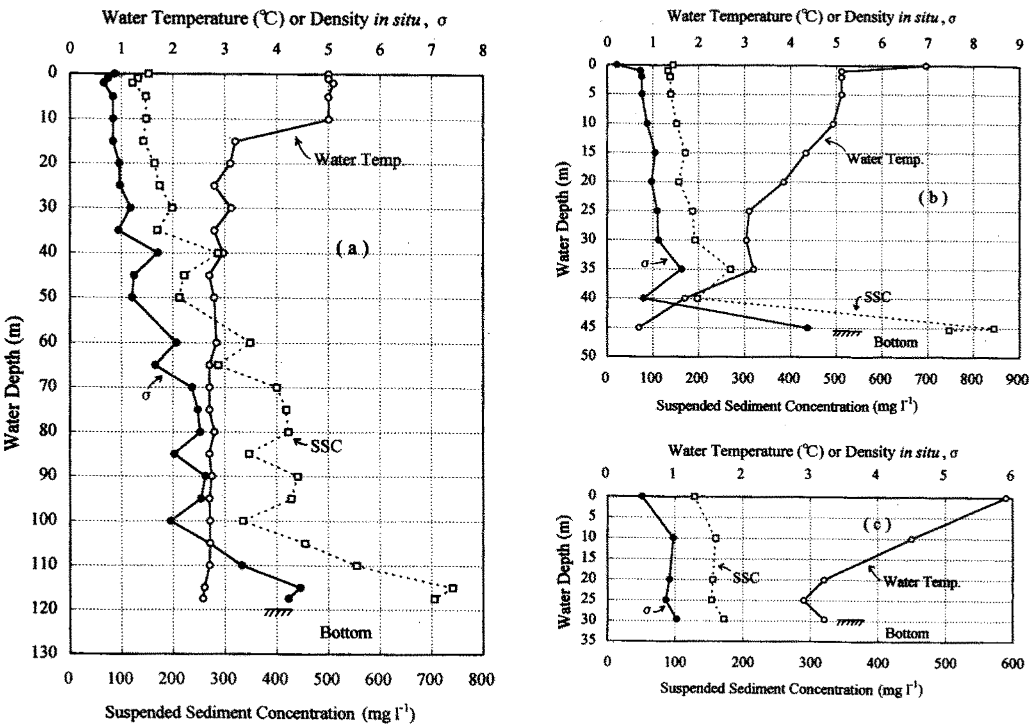

Fig. 4. Vertical profiles of water temperature, suspended sediment concentration (SSC) and density *in situ* σ at (a) site B, (b) site G and (c) site G' (50 m southwest of site G). The profiles were obtained (a) at 7 : 09−8 : 03 on 26 May 1995, (b) at 8 : 31−8 : 55 on 26 May 1995 and (c) at 9 : 34−9 : 42 on 27 May 1995.

Lake currents driven by a valley wind are likely to prevail in the surface layer toward the glacier terminus because of the large fetch over the lake (Fig. 2) ; the wind-driven currents could transport the radiative heat actively for melting the lower (subaqueous) part of the glacier terminal cliff.

The temperature distribution at site G (Fig. 4b) indicates the heating near the surface by solar radiation and an isothermal condition (about 5 °C) at depths of 0.5−10 m as at site B. At depths of 10−35 m, the temperature is higher than that at site B, whereas at more than 35 m, it decreases to 0.7 °C near the bottom. The higher temperature at 10−35 m depth probably results from the uplake heat transport by wind-driven currents, consequently generating the downwind *setup*. At depths less than 40 m, SSC is numerically like that at site B, but increases greatly at more than 40 m up to the maximum 844 mg/l at 0.3 m above the bottom. The cold and turbid water near the bottom is judged to indicate *sediment-laden underflows* produced by the glacier-melt water discharged from a mouth of englacial tunnels. The sediment-laden underflows could go downslope to the deepest zone of Tsho Rolpa Lake, since the meltwater density (σ=4.36 or ρ= 1000.436 kg/m^3) at site G is higher than or comparable to water densities ($0.86<\sigma<4.45$ or $1000.086<\rho<1000.445$ kg/m^3) above the bottom of site B (Fig. 4a), and also the suspended sediment in the meltwater is rather fine (almost clay and silt) (Yamada, 1996 ; for dynamic motions of sediment-laden underflow, see Chikita, 1989 and Chikita *et al.*, 1996). Actually, the pycnally unstable layer of relatively low temperature and SSC just above the bottom of site B can be produced by such turbulent shear flows as sediment-laden underflows (Chikita, 1990).

The meltwater discharge from *one* subaqueous mouth is obvious by comparison with the profiles at site G', 50 m off site G or at the middle of the glacier terminal cliff in transect (Fig. 4c ; see Fig. 2). Site G', shallower than site G, has no cold and turbid water near the bottom. The subaqueous tunnel mouth was probably grown by the selective ice-melt at the terminus from the original meltwater discharging. The thickness of the cold and turbid bottom layer at site G (Fig. 4b) suggests that the mouth is about 10 m in height.

Vertical temperature and SSC profiles at sites C, D and E indicated the existence of relatively cold and turbid layer on the bottom as those at sites B and G, thus evidencing the downslope motion of meltwater by the underflows (see Fig. 2 for the site location). Site A, however, did not have the specific bottom layer. The downslope water motion by underflows can thus be traced from near the subaqueous mouth to the deepest zone at more than about 110 m, which is below the bottom of site A (107.4 m deep). This is because common density underflows, driven by the product of the downslope component of the buoyant gravity and the flow thickness, can reach to the deepest point, as far as they hold sediment in suspension. Suspended sediment supplied into Tsho Rolpa Lake is mostly silt and clay with low settling velocity (Sakai, 1995 ; Yamada, 1996). The sediment-laden underflows could thus continue by keeping some sediment suspended for a long time, even if they are weakened by deposition and *bifurcation* on the way to the deepest point (131 m deep). After reaching to the deepest point, the underflows could move for some time by inertia, because of the low settling velocity of suspended sediment. The SSC profile near the bottom of site B (Fig. 4a) suggests that the upper level of the suspension movement is about 110 m deep, corresponding to the upper interface of the underflows.

Four local maximums of SSC or σ at depths of 40−100 m at site B (Fig. 4a), indicating the pycnal instability, were probably produced by shear flows such as density interflows, *i.e.* the horizontal intrusions of turbid meltwater supplied from the subaqueous tunnel mouth. This means that the sediment-laden underflows were bifurcated into four interflows on the way to the deepest zone. The bifurcation phenomenon will be schematically depicted later (Fig. 7). It is unknown, however, if the interflows could reach to the downlake end to exert some effect on thermal conditions at the bottom of the terminal moraine. Dynamic behaviors of the interflows should be investigated minutely by more data collection.

3-3. *Temporal Variations of Water Temperature*

Fig. 5 shows time series of water temperature at sites A and G, and wind speed and solar radiation at site M at 1 h intervals for a period 25 May to 27 May 1995. Consequently, the temperature record only continued within the 3 days, but indicated clear diurnal variations at depths of 0.1 m and 20 m at either site. At 20 m depth, the temperature at site G is consistently higher than that at site A except for the time period of 6 : 00−12 : 00 on 27 May. This suggests the radiative-heat transport toward the glacier terminus by wind-driven currents and consequently

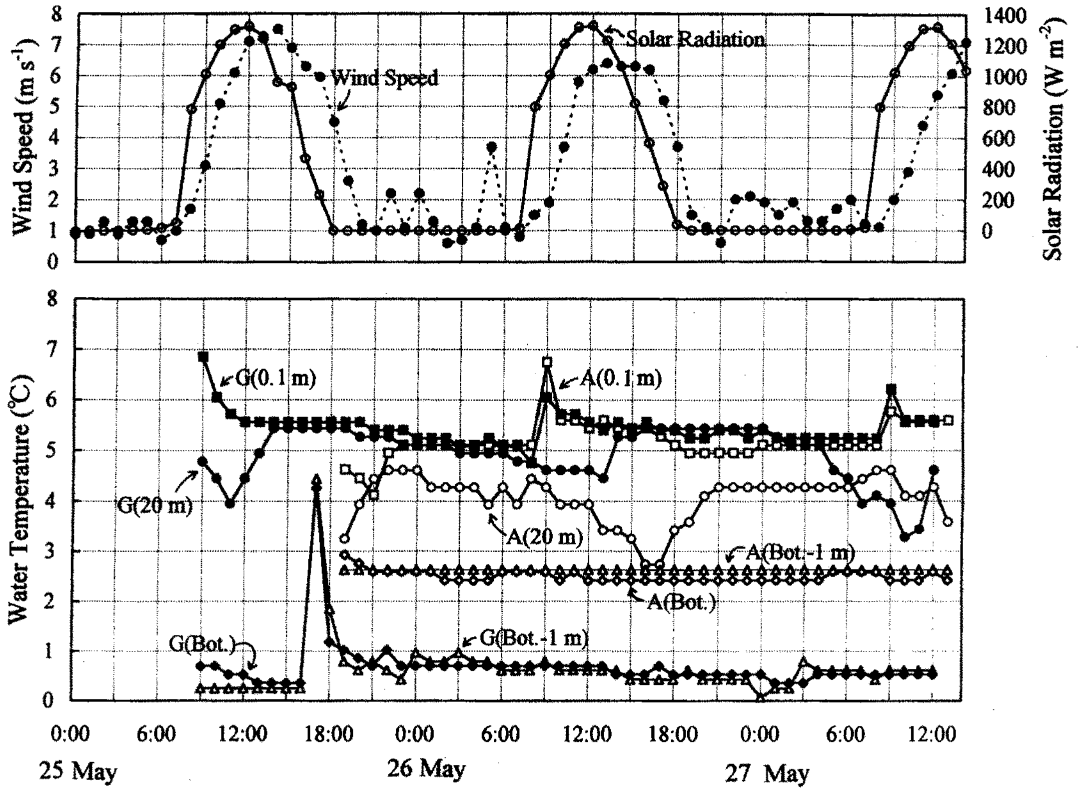

Fig. 5. Time series of water temperature at depths of 0.1 m and 20 m, at the bottom and at 1 m above the bottom (sites A and G), and wind speed and solar radiation at site M for 25–27 May 1995.

the continuous appearance of the heated water near the terminus. As typified by the record for 7 : 00–17 : 00 on 26 May, the temperature increase at site G from 13 : 00 is preceded by a relatively great decrease of temperature at site A from 8 : 00 and an increase of wind speed from 7 : 00. The temperature decrease at site A probably resulted from the transport of relatively cold water from downlake to compensate for the warm water which wind-driven currents transported toward the glacier terminus. The delayed increase at site G may indicate the slow appearance of the warm water transported by wind-driven currents. These suggest that wind-driven currents control the thermal structure of the surface layer at less than about 20 m.

The downwelling of warm (about 5 °C) surface water could occur at the glacier terminus during the daytime setup. This probably induces the cooling of the surface water by a direct contact of the glacier ice. The cooled water would subsequently intrude as density interflows at depths of 20–35 m, *i.e.* at the lower part of the isopycnal surface layer (see Fig. 4a). The vertical water circulation generated by a valley wind may thus be completed by the upwelling of the cooled water at the downlake end.

It is noted in Fig. 5 that at the bottom of site A (107.4 m deep), temperature varied diurnally with a maximum at 6 : 00–7 : 00 in spite of the small fluctuation. This diurnal variation could correspond to that of meltwater temperature at the bottom or 1 m above the bottom at site G. The maximums at site A were delayed by 6 to7 hours for those at 1 m above the bottom of site G ; this delay gives the mean speed of underflows at 4.4–5.1 cm/s, by considering the distance (1.1 km) between sites G and A (see Fig. 2). Hence, Reynolds number, $Re = UH/\nu$ and densimetric Froude number, $Fr = U/(gH\Delta\rho/\rho_w)^{1/2}$ of the underflows can be calculated, where U is the mean speed, H is the flow thickness, ν is the kinematic viscosity, g is the acceleration due to gravity, $\Delta\rho$ is $\rho_f - \rho$ (ρ_f, the underflow density ; ρ, the surrounding water density) and ρ_w is the clear water density. $Re=1.9\times10^5-2.1\times10^5$ and $Fr=0.38-0.44$ were here obtained, giving $U=0.044-0.051$ m/s, $H=7$ m, $\nu=1.65\times10^{-6}$ m²/s, $g=9.8$ m/s², $\rho_w=1000.0$ kg/m³, $\rho_f=1000.4$ kg/m³ and $\rho=1000.2$ kg/m³ from Fig. 4a. This indicates that the underflows are turbulent and subcritical (cf. Chikita, 1989, Chikita *et al.*, 1991).

At 1 m above the bottom, temperature kept constant. This may indicate no water motion nor effects of sediment-laden underflows on the thermal condition probably because of the level higher than the upper interface of the underflows. This is compatible with the result that a meltwater motion by underflows is restricted to the bottom layers from near the glacier terminus to the deepest point to around the bottom level of site A (about 110 m deep) (Figs. 4a and 4b).

A temperature peak of 4.2−4.3 °C appeared simultaneously at the bottom and at 1 m above the bottom of site G at 17 : 00 on 25 May. This peak was possibly produced by the short-term discharge of relatively warm meltwater or the strong downwelling of relatively warm surface water during the leeward setup. At 0.1 m depth of sites A and G, daily temperature peaks appeared simultaneously at about 9 : 00. This indicates a direct effect of solar radiation on the still water at near the lake surface before the beginning of a valley wind.

Fig. 6 shows FFT power spectra calculated for time series of water temperature at sites A and G. The spectra at 1 m above the bottom of site G have significant peaks at periods of 0.95 h (57 min), 0.47 h (28 min), 0.33 h (20 min), 0.25 h (15 min), 0.17 h (10 min), 0.12 h (7 min) and 0.083 h (5 min), thus showing the fundamental (about 1 h) or higher mode. These peaks possibly indicate high frequencies in the diurnal variation (Fig. 5), though a peak of a 24 h (or 1440 min) period cannot appear from the 3-day data.

The spectrum at 20 m depth of site A is analogous to that at 1 m above the bottom of site G in having same periods of 28 min, 10 min, 7 min and 5 min. This suggests the intrusion of the downwelling cooled water into the 20-m depth of site A (see Fig. 7). The spectrum at 20 m depth of site G is similar to that at 20 m depth of site A, showing some peaks at same

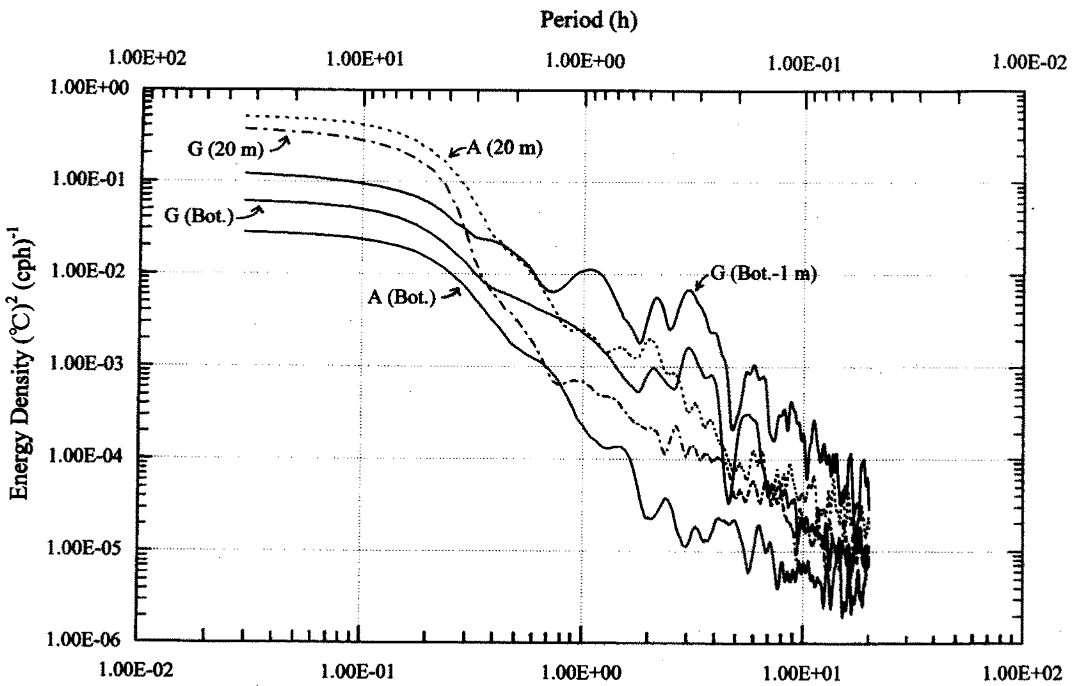

Fig. 6. Power spectra of water temperature at site A (20 m depth and bottom) and site G (20 m depth, bottom and 1 m above the bottom) calculated by the FFT (Fast Fourier Transform) method.

periods. The G-20 m peaks, however, are rather unclear except the peak at 0.38 h (23 min). This suggests the continuous intrusion of cooled surface water into the 20 m depth of site G.

The spectrum at the bottom of site A has peaks at periods of 0.68 h (41 min), 0.42 h (25 min), 0.23 h (14 min), 0.20 h (12 min) and 0.17 h (10 min). These peaks does not correspond to those at 20 m depth of site A and at 1 m above the bottom of site G. This suggests that a thermal condition at the bottom of site A is not directly affected by discharging meltwater but by the lake water entrained by sediment-laden underflows on the way to the deepest zone (Fig. 7). Before reaching to the deepest zone, the underflows could be weakened by the entrainment of the surrounding lake water and the bifurcation into density interflows. The periodicity of meltwater temperature is thus considered to have been untraceable at the bottom of site A.

The bottom temperature between sites G and A, anyhow, could be controlled by the dynamic behaviors of sediment-laden underflows. The underflows tend to transport relatively cold water and deposit their suspended sediment on the lake bottom. As the deposit thickness increases, the temperature gradient between the bottom water and underground ice decreases. The sediment deposition and cold water transport thus decreases the bottom heat flux. Hence, the underflows would not exercise a considerable effect on the underground ice-melt except at near the subaqueous tunnel mouth, where the flow energy or turbulent heat diffusion is enough. It is here difficult to evaluate the heat flux with respect to the underground ice melt, since spatial distributions of the sediment thickness and ice are unknown ; the underground structure and present sedimentation rate could be specified by using a seismic profiler (*e.g.*, see Nakao and Yamashita, 1978, Handa *et al.*, 1987) and sediment traps, respectively.

3-4. Rate of Lake-Basin Expansion

The maximum rate of the lake-basin expansion has so far been observed at the glacier terminal cliff. It is because the *carving* of glacier ice at the terminus occurs by the relatively great ice-melt at the lower part directly contacted by lake water. The carving means the collapse of ice body at the cliff-shaped glacier terminus along large splits like crevasse. According to topographic data of Kadota (1994), the glacier terminus above the lake surface receded by 80 m at maximum (50 m averaged in transect) for a period 18 September 1993 to 20 June 1994, and by 120 m at maximum on 27 June 1994, due to the carving. A pond on the glacier disappeared after the large collapse (Kadota, 1994). At about 16 : 40 on 25 May 1995, the carving generated a surface surge with the wave height of about 20 cm and a period of 26 sec. The rate of lake-basin expansion at the terminus is thus 29−71 cm/d at maximum or 18 cm/d on average. The radiative heat transport toward the terminus by wind-driven currents could increase the melting of the subaqueous lower ice and consequently enhance the carving of the glacier.

The outburst potentiality of Tsho Rolpa Lake is known by quantifying ice-melt conditions in the terminal moraine subject to the lake-water pressure. The terminal moraine partially contains the fossil ice, mostly distributing in the downlake region less than 20 m deep (Fig. 2 ; see Yamada, 1996). The lake bottom at near site M (Fig. 2) subsided by 48.1 cm on average for a period 14 November 1993 to 3 October 1995, thus the mean daily rate of 0.064 cm/d (Yamada, 1996). In the downlake region, in addition to a contact with the lake water heated by solar radiation, the surface discharge at site R (~8 m^3/s) could exalt the underground ice-melt by inducing *slope currents*, which is generated by a difference of water head between the outlet and farther lake surface(Chikita *et al.*, 1985).

4. Conclusions

In this study, the role of lake hydrodynamics on thermal conditions at the bottom and the consequent rate of the lake-basin expansion were documented by observing the meteorology, lake water properties and lake basin topography. Fig. 7 shows a schematic diagram of lake hydrodynamics and its effect on the lake-basin expansion obtained from the present observation. A strong valley wind blowing typically at 10 : 00−19 : 00 could efficiently produce wind-driven currents to transport the radiative heat to the glacier terminus at the uplake end and then to downwell warm surface water at the terminus. The surface water contacted by the glacier ice is cooled during the downwelling, and subsequently intrudes into the lower part (25−35 m depth) of the isopycnal layer as density interflows. In the longitudinal section of the lake, the valley-wind shear thus tends to generate vertical water circulation in the isopycnal layer from the surface to about 35 m in depth (see Fig. 4). The

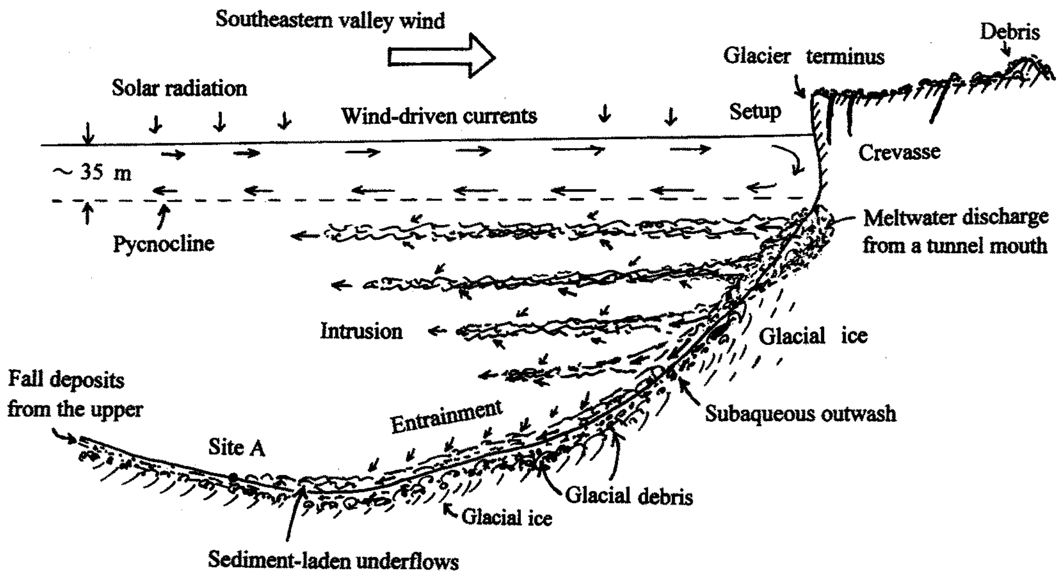

Fig. 7. Schematic of lake currents and their sedimentation which affect the ice melt on or below the bottom basin at uplake from around site A (midlake). The upper interface of sediment-laden underflows is at around the level of the bottom at site A.

downwelling of warm surface water increases the ice-melt at the lower part of the glacier terminal cliff, thus enhancing the ice carving at the upper aerial part.

The discharge of glacier-melt water (probably, at 0°C) could produce a subaqueous tunnel mouth by the relatively large ice-melt at the lower part of the glacier terminus. The meltwater involves much fine-grained sediment of silt and clay (Yamada, 1996), and consequently generates sediment-laden underflows at near the mouth. During the downslope motion, the underflows deposit their suspended sediment on the bottom, which may form the subaqueous outwash involving sediment sorting (Edwards, 1986, Chikita, 1992). The underflows simultaneously entrain the relatively warm and clear water at the upper interface. These could decrease the kinetic energy of the underflows and make unstable their interior density structure relative to the surrounding water density. The density instability tends to produce the bifurcation of underflows into some interflows (Fukuoka and Fukushima, 1980). The maximums of suspended sediment concentration below the isopycnal layer probably result from the intrusion of relatively turbid water by the interflows. However, it is unknown to what extent the interflows exert an effect on the bottom temperature at the downlake end corresponding to the intrusive depth. It is because interflows tends to gradually lose the kinetic energy with increasing flow thickness by entraining the ambient water. Suspended sediment in the interflows could finally settle down to the bottom as fall deposits. The deposition, however, is probably slight in amount compared with sedimentation by sediment-laden underflows.

Sediment-laden underflows are traceable up to the deepest zone more than 110 m in depth. This means that the bottom temperature from near the subaqueous tunnel month to the midlake (at or around site A) could be determined by water motions of the underflows. Sediment-laden underflows, however, probably exert no considerable effect on the ice-melt below the bottom, because during the downslope motion, they tend to lose the kinetic energy effectively by depositing suspended sediment, entraining the surrounding water of relatively low turbidity and bifurcating themselves into some interflows. Their fully turbulent heat diffusion, thus, is not expected. Also, the sediment deposition could decrease the bottom heat flux by decreasing temperature gradient between the bottom water and underground ice.

The lake water density depends on suspended sediment concentration rather than water temperature. The suspended sediment is mostly clay and silt, which is transported largely by the sediment-laden underflows and interflows ; The debris on the moraines adjacent to the lake is rather coarse, though its collapse into the lake is frequent. The density structure in the lake is thus dominated by the two kinds of density currents. The wind-driven currents and subsequent downwelling and countercurrents, *i.e.* the vertical water circulation during the leeward setup could exert a considerable effect on the lake basin expansion, especially at the glacier terminus.

Information on sedimentary structure and glacial ice distribution below the bottom is necessary to evaluate heat flux at the lake bottom. Numerical simulation by a modeled lake, where sedimentation is taken into account, could then clarify systematic relationship among the basin expansion, glacier-melt discharge and lake hydrodynamics.

Acknowledgments

We are grateful to all associated members of CREH (Cryosphere Research Expedition of Himalaya) for their help to prepare for the field work. This study was made as one of the activities of CREH (Supervisor, Prof. U. Ageta, Nagoya University) financially supported by the grant-in-aid of the International Scientific Research, No. 06041051, the Ministry of Education, Sciences, Sports and Culture of Japan, and also as a GLOF (Glacier Lake Outburst Flood) research program assisted by JICA (Japan International Cooperation Agency).

References

1. Chikita, K., Hattori, M. and Hagiwara, E. (1985) : A field study on river-induced currents — an intermountain lake, Lake Okotanpe, Hokkaido. Jpn. J. Limnol., **46**, 256–267.
2. Chikita, K. (1989) : A field study on turbidity currents initiated from spring runoffs. Water Res. Res., **25**, 257–271.
3. Chikita, K. (1990) : Sedimentation by river-induced turbidity currents : Field measurements and interpretation. Sedimentology, **37**, 891–905.
4. Chikita, K., Yonemitsu, N. and Yoshida, M. (1991) : Dynamic processes of sedimentation in a glacier-fed lake, Peyto Lake, Alberta, Canada. Jpn. J. Limnol., **52**, 27–43.
5. Chikita, K. (1992) : Dynamic processes of sedimentation by river-induced turbidity currents. II. Application of a two -dimensional, advective diffusion model. Trans., Jpn. Geomorph. Union, **13**, 1–18.
6. Chikita, K., Smith, N.D., Yonemitsu, N. and Perez-Arlucea, M. (1996) : Dynamics of sediment-laden underflows passing over a subaqueous sill : glacier-fed Peyto Lake, Alberta, Canada. Sedimentology, **43**, 865–875.
7. Edwards, M. (1986) : Glacial environments. In Sedimentary Environments and Facies, ed. H.G. Reading, Chapter 13, 445–470.
8. Fukuoka, S. and Fukushima, Y. (1980) : On dynamic behavior of the head of the gravity current in a stratified reservoir. Proc. Second Intern. Symp. on Stratified Flows, 24–27, Norwegian Inst. Technol., Trondheim, Norway.
9. Handa, N., Kanari, S. Inouchi, Y. and Okino, T. (1987) : A handbook for lake surveys. Kokon-Shoin, 215pp. (in Japanese)
10. Jones, P.D., Wigley, T.M.L. and Wright, P.B. (1986) : Global temperature variations between 1861 and 1984. Nature, **322**, 430–434.
11. Kadota, T. (1994) : Report for the field investigation on the Tsho Rolpa Glacier Lake, Rolwaling Valley, February 1993–June 1994. WECS N551.489KAD.
12. Mool, K., Kadota, T., Maskey, P.R., Pokharel, S. and Joshi, S. (1993) : Interim report on the field investigation on the Tsho Rolpa Glacier Lake, Rolwaling Valley. WECS Report No. 3/4/021193/1/1, Seq. No. 436.
13. Nakao, K. and Yamashita, T. (1978) : Sedimentary structure in Lake Abashiri inferred from continuous seismic profiling using "UNIBOOM". Jpn. J. Limnol., **39**, 61–65 (in Japanese with English abstract).
14. Sakai, A. (1995) : Thermal characteristics of the Tsho Rolpa Glacier Lake. M. Sc. Thesis, Hokkaido University, 66 pp. (in Japanese).
15. Yamada, T. (1993) : Glacier lakes and their outburst floods in the Nepal Himalaya. WECS/JICA, Nepal, 37pp.
16. Yamada, T. (1996) : Report on the investigations of Tsho Rolpa Glacier Lake, Rolwaling Valley. WECS/JICA, Nepal, 129 pp.